Ionic Currents Underlying Fast Action Potentials in the Obliquely Striated Muscle Cells of the Octopus Arm

Dan Rokni and Binyamin Hochner

Ionic Currents Underlying Fast Action Potentials in the Obliquely Striated Muscle Cells of the Octopus Arm

DAN ROKNI AND BINYAMIN HOCHNER
Department of Neurobiology, Institute of Life Sciences, and the Interdisciplinary Center for Neuronal Computation, Hebrew University, Jerusalem 91904, Israel

Rokni, Dan, and Binyamin Hochner. Ionic currents underlying fast action potentials in the obliquely striated muscle cells of the octopus arm. *J Neurophysiol* 88: 3386–3397, 2002; 10.1152/jn.00383.2002. The octopus arm provides a unique model for neuromuscular systems of flexible appendages. We previously reported the electrical compactness of the arm muscle cells and their rich excitable properties ranging from fast oscillations to overshooting action potentials. Here we characterize the voltage-activated ionic currents in the muscle cell membrane. We found three depolarization-activated ionic currents: *1*) a high-voltage-activated L-type Ca^{2+} current, which began activating at approximately -35 mV, was eliminated when Ca^{2+} was substituted by Mg^{2+}, was blocked by nifedipine, and showed Ca^{2+}-dependent inactivation. This current had very rapid activation kinetics (peaked within milliseconds) and slow inactivation kinetics (τ in the order of 50 ms). *2*) A delayed rectifier K^+ current that was totally blocked by 10 mM TEA and partially blocked by 10 mM 4-aminopyridine (4AP). This current exhibited relatively slow activation kinetics (τ in the order of 15 ms) and inactivated only partially with a time constant of ~150 ms. And *3*) a transient A-type K^+ current that was totally blocked by 10 mM 4AP and was partially blocked by 10 mM TEA. This current exhibited very fast activation kinetics (peaked within milliseconds) and inactivated with a time constant in the order of 60 ms. Inactivation of the A-type current was almost complete at -40 mV. No voltage-dependent Na^+ current was found in these cells. The octopus arm muscle cells generate fast (~3 ms) overshooting spikes in physiological conditions that are carried by a slowly inactivating L-type Ca^{2+} current.

INTRODUCTION

Complexity in the control of arm movement is directly related to the number of degrees of freedom of the arm. The octopus arm provides an extreme case of an arm with virtually unlimited degrees of freedom that can elongate, shorten, bend, or twist at any point. The octopus arm thus provides a unique natural model system for unraveling the motor control of flexible arms (Gutfreund et al. 1996, 1998; Matzner et al. 2000; Sumbre et al. 2001).

Like other cephalopod tentacles, vertebrate tongues and the elephant trunk, the octopus arm lacks any form of rigid skeleton, and it is the muscles that supply skeletal support for movement as well as generating force. These flexible structures are composed mainly of incompressible muscle tissue and therefore remain constant in volume. Therefore they were termed muscular hydrostats (Kier and Smith 1985). This biomechanical constraint causes muscles acting in three orthogonal directions to work against each other, thus generating both the stiffness and the contraction that are required for movement.

Apart from muscles of the chromatophors (Bone et al. 1995), little is known about the physiology of cephalopod muscles. This is partly due to the small diameter of cephalopod muscle fibers that makes them inconvenient for electrophysiological experiments (length: 0.5–2 mm, diameter: ~10 μm) (Bone et al. 1995; Kier 1985). Although the mechanical responses of cephalopod mantle muscles and their morphology have been analyzed (Lowy and Millman 1961; Milligan et al. 1997; O'Dor 1988; Prosser and Young 1937; Rogers et al. 1997), there is only little information about the ionic basis of excitation-contraction mechanisms in cephalopod muscles, generally, and octopus arm muscle fibers, in particular (see Gilly et al. 1996; Rogers et al. 1997).

Matzner et al. (2000) have shown that octopus arm muscle cells exhibit a variety of regenerative responses when stimulated directly with current or activated by synaptic inputs. These regenerative responses are all rapid and range from neuron-like spikes to fast voltage oscillations. Here we characterize the voltage dependent ionic currents that participate in the generation of these regenerative responses in the octopus arm muscle cells to reveal their electrical transformation properties.

METHODS

Specimens of *Octopus vulgaris* were collected by local fishermen in the Mediterranean Sea or imported from the Stazione Zoologica, Naples, Italy. The octopuses were kept individually in aquaria of artificial seawater, which circulated through a closed system of biological filters. Aquaria were regulated to 17°C, 12 h light/dark cycle, and the octopuses were fed fish meat once a day. These conditions enabled us to keep the octopuses for ≤6 mo, during which they gained weight at what seemed to be a normal rate.

The animals were anesthetized in cold seawater (4–10°C) containing 2% ethanol. A short segment, 1–3 cm long, was dissected from the middle of the arm and kept in artificial seawater (ASW; see following text) at ~10°C. Experiments were carried out at room temperature (20–24°).

Address reprint requests to: B. Hochner (E-mail: bennyh@lobster.ls.huji.ac.il).

Dissociated muscle fibers

Dissociated muscle fibers were prepared according to the method of Brezina et al. (1994a). A small piece of arm muscle was taken under microscopic control from a designated area of the intrinsic musculature of the arm. The tissue was incubated at 25–30°C for 4–6 h in 0.2% collagenase (Sigma type I) dissolved in L15 culture medium (Biological Industries, Bet Haemek, Israel) adjusted to the concentration of salts in seawater. The enzymatic treatment was terminated by rinsing with L15. The tissue was then triturated manually until an appreciable concentration of dissociated muscle cells could be detected in the supernatant. These cells were kept in 17°C for ≤5 days; their physiological properties did not appear to deteriorate during this period. For electrophysiological experiments, an aliquot of the cells was transferred to a plastic petri dish mounted on an inverted microscope. The cells settled on the bottom of the dish within a few minutes.

Electrophysiological recordings

The electrical properties of the isolated muscle cells were investigated in the whole cell discontinuous voltage-clamp mode using Axoclamp 2B (Axon Instruments). Sampling rate of the discontinuous voltage-clamp was 5–10 kHz. Electrodes were pulled on a pp-830 puller (Narishige, Japan) using a two-step procedure and had a DC resistance of 2–4 MΩ. In some cases, there was a discrepancy of ≤10 mV between the command potential and the actual measured potential. The experiment was discarded if the difference became >10 mV. However, measured potentials were always used for data analysis.

At the beginning of the experiment, the muscle fibers usually contracted during depolarizing commands. Thus fibers were much shorter by the end of an experiment than at the beginning. The contractions did not impair the seal, and there were no motion artifacts, possibly because the muscle cells were strongly attached only to the electrode.

Solutions and drugs

Normal artificial seawater (ASW) contained (in mM) 460 NaCl, 10 KCl, 55 MgCl$_2$, 11 CaCl$_2$, 10 glucose, and 10 HEPES, pH 7.6 (adjusted with NaOH). Other solutions were made using equimolar substitutions of this basic formula. The patch pipettes were filled with the following internal solution (in mM): 465 K-gluconate, 2 MgCl$_2$, 1 CaCl$_2$, 10 K-EGTA, 5 Na$_2$ATP, 0.5 Na$_2$GTP, and 50 HEPES, buffered to pH 7.2 with KOH.

CA^{2+} CHANNEL CHARACTERIZATION.   Ba-ASW contained 11 mM BaCl$_2$ instead of CaCl$_2$, and Mg-ASW contained 11 mM MgCl$_2$ in addition to the normal 55 mM and no CaCl$_2$. Unless otherwise indicated, all Ca^{2+} channel characterization experiments were conducted in ASW in which Na$^+$ was replaced with TEA and 10 mM 4-aminopyridine (4AP; Fluka or Sigma) was added. A stock solution of 10 mM nifedipine (Sigma) was prepared in DMSO and dissolved in the bath solution to reach a final concentration of 20 μM. The bath solution therefore contained 0.2% DMSO, which by itself had no effect on Ca^{2+} currents. In some experiments, ≤9 μM TTX (Sigma) was added to the bathing solution. K-gluconate in the internal solution was substituted with CsCl to block K$^+$ currents internally.

K$^+$ CHANNEL CHARACTERIZATION.   All experiments were carried out in Mg-ASW to block Ca^{2+} currents. TEA substituted equimolar amount of the NaCl to block delayed rectifier K$^+$ currents, and 4AP was added to block transient K$^+$ currents.

Drug administration

A slow and continuous perfusion system was used to replace the 2 ml solution in the petri dish with fresh ASW at a rate of ~4 ml/min. Drugs were applied as previously published (Matzner et al. 2000). The area of recording was constantly superfused via a polyethylene tip drawn to a diameter of ~100 μm mounted on a micromanipulator and placed <2 mm from the cell. Hydrostatic pressure was used to drive four different solutions through polyethylene tubing into the drawn tip. The small free space at the tip enabled exchange of solutions in a few seconds. Solenoid-driven valves were used to switch between different solutions, enabling solution changes within seconds. When drugs were not applied, ASW was driven through this system to prevent changes in flow during the experiment.

Data storage and analysis

A software program written in Labview was used to store and analyze data digitally. Data were sampled at 20 kHz. Linear leakage conductance was evaluated by applying a 10-mV voltage step from a holding potential of between −70 and −90 mV. This conductance was then linearly scaled and subtracted from all current measurements post facto. However, leakage current was typically <5–10% of the ionic currents measured.

Sigmoidal activation curves were fitted using a Boltzman function of the following form

$$g(V) = g_{max}/(1 + e^{-(V-V_{1/2})/k}) \tag{1}$$

where $g(V)$ is the conductance, g_{max} is the maximum conductance, $V_{1/2}$ is the voltage of half activation, and k is the slope factor. Sigmoidal inactivation curves were fitted using a Boltzman function of the following form

$$g_r(V) = 1 - a/(1 + e^{-(V-V_{1/2})/k}) \tag{2}$$

where g_r is the relative conductance and a is the maximal extent of inactivation.

Mean Boltzman functions for data pooled from several experiments were generated using the average parameters of the individual Boltzman curves (k, $v_{1/2}$, and g_{max} or a). Capacitance was measured by integrating the capacitive current of a 10-mV voltage command at a low clamping gain and dividing it by the amplitude of the voltage step.

RESULTS

The passive electrical properties of the muscle cells were examined using whole cell voltage-clamp recordings. Average values for input resistance and for membrane capacitance were 409 ± 267 (SD) MΩ ($n = 19$) and 0.19 ± 0.05 nF ($n = 19$), respectively.

Current injection during whole cell current-clamp recordings yielded a variety of electrical responses, ranging from overshooting action potentials and fast oscillatory responses to plateau potentials (Fig. 1, *A–D*) (see also Matzner et al. 2000).

Pharmacological experiments were first conducted under current-clamp conditions to identify the ionic mechanisms underlying the regenerative electrical activities of the octopus arm muscle cells. Figure 1*E* shows an example of an experiment in which spikes were blocked by 10 μM nifedipine but were insensitive to 4.5 μM TTX (TTX concentrations of ≤9 μM did not block spikes). This concentration is more than an order of magnitude higher than the concentration sufficient to block Na$^+$ channels in squid mantle muscle cells (Gilly et al. 1996). These spikes thus appear to result mainly from a Ca^{2+} current.

Characterization of the inward current

We used the discontinuous single electrode voltage-clamp technique in the whole cell configuration to characterize the inward current responsible for the spiking activity of the arm
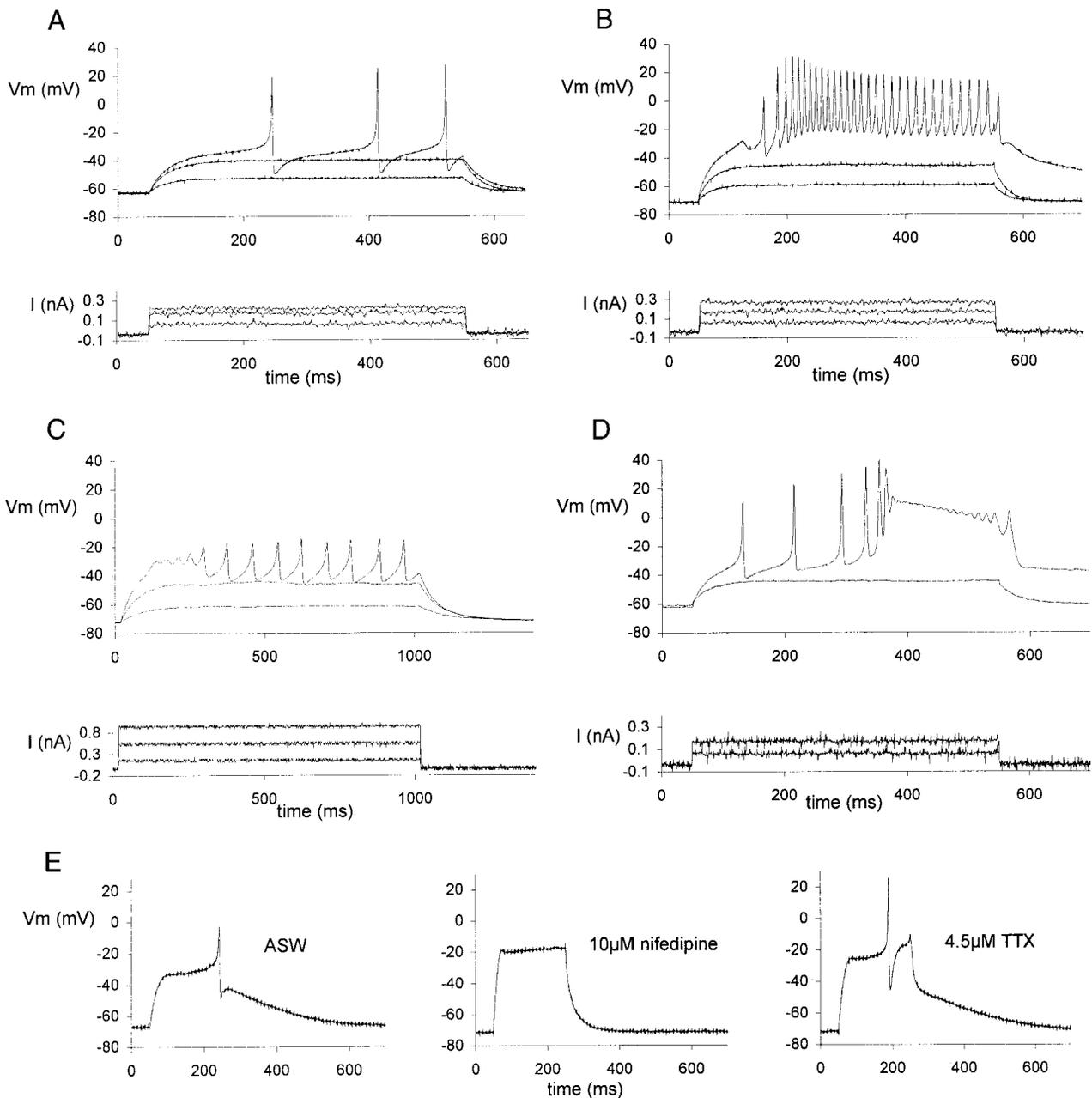
FIG. 1. Current injections to dissociated muscle fibers of the octopus arm reveal a variety of electrical responses activated at relatively high depolarization. *A*: typical neuron-like action potentials seen in most of the muscle fibers. *B*: a high-amplitude "oscillatory" response shows accelerating fluctuations in membrane potential. *C*: low-amplitude "oscillatory" response. *D*: a plateau potential. *E*: a current clamp experiment showing that the spiking activity of the muscle cell is blocked by 10 μM nifedipine but is not affected by application of 4.5 μM TTX. The sequence of the experiment is from left to right. 0.5 nA was injected in artificial seawater (ASW), 1.3 nA in nifedipine, and 0.8 nA in TTX. Duration of the current step was 200 ms.

muscle cells. Neither TTX nor Na$^+$ substitution (data not shown) affected the inward current and use of normal Na$^+$, Ca^{2+}-free extracellular solutions also failed to reveal a Na$^+$ current. Conditions were thus held suitable for characterizing Ca^{2+} currents and experiments were performed in low Na$^+$ ASW containing 460 mM TEA and 10 mM 4AP, and with Cs$^+$ instead of K$^+$ in the intracellular solution to minimize outward current contamination.

Applying depolarizing voltage steps from a holding potential of −70 mV revealed a fast-activating, slow-inactivating inward current (Fig. 2*A1*). This is most probably a Ca^{2+} current

because *1*) it was insensitive to TTX (data not shown), *2*) persisted in low Na$^+$ high TEA ASW, *3*) totally disappeared by substituting the extracellular Ca^{2+} with Mg^{2+} (Fig. 2*B*), and *4*) it was mostly blocked by applying 20 μM nifedipine to the bath solution (Fig. 2*C*). This Ca^{2+} current resembles the L-type Ca^{2+} current (Carbone and Swandulla 1989; Hille 1992) as it shows high activation threshold (approximately −35 mV; Fig. 2, *A2*, *B2*, and *C2*) and slow inactivation and is blocked by nifedipine, a known high-voltage-activated (HVA) L-type Ca^{2+} channel blocker (Brezina et al. 1994c; Carbone and Swandulla 1989; Yeoman et al. 1999).
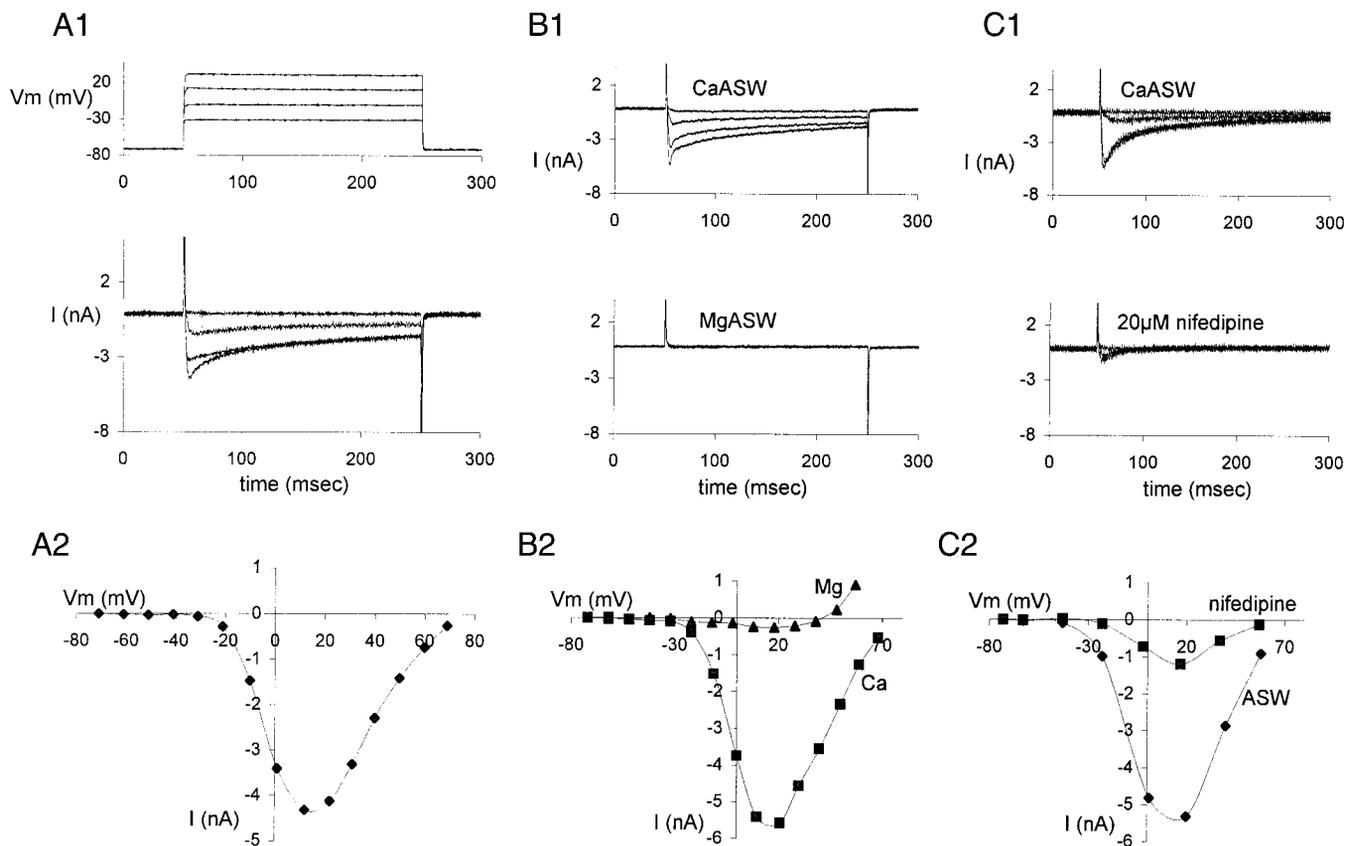
FIG. 2. An L-type Ca^{2+} current is revealed in a typical voltage clamp experiment with 460 mM TEA and 10 mM 4AP in the extracellular medium and Cs^+ in the intracellular solution. *A1*: depolarizing voltage steps from a holding potential of −70 mV elicited a fast-activating slow-inactivating inward current. The current usually did not inactivate fully within the 200-ms depolarizing step. *A2*: peak current-voltage relationship of the inward current in the same cell as in *A*. Current began activating at voltages more positive than −40 mV, peaked at about +15 mV, and extrapolated to reversal above +70 mV. *B* and *C*: pharmacological characterization of the inward current. *B1*: total block of the inward current when using Mg-ASW as the bathing solution. Voltage steps to −20, −10, 0, and 10 mV from a holding potential of −70 mV. *B2*: the *I-V* curves of the Ca^{2+} current in both solutions (peak currents are plotted). *C1*: 20 μM nifedipine blocked the inward current to <0.25 of the control value. Voltage steps to −40, −20, 0, and 20 mV from a holding potential of −70 mV. *C2*: *I-V* curves before and after application of the drug (peak currents are plotted).

Ca vs. Ba currents

Substituting Ba^{2+} for Ca^{2+} usually increases the amplitude and slows inactivation of L-type Ca^{2+} currents (Brezina et al. 1994c). Surprisingly, although the other properties of the inward current here seem typical for an L-type current, (high activation, sensitivity to nifedipine and kinetics) Ba^{2+} substitution resulted in smaller inward current when using identical voltage steps throughout the whole voltage range (Fig. 3). This was evident in all experiments. Peak amplitudes of Ca^{2+} currents averaged 8.1 ± 2.9 nA ($n = 5$), while peak amplitudes of currents elicited in ASW containing 11 mM Ba^{2+} averaged 6.1 ± 1.6 nA ($n = 5$). The average difference between peak Ca^{2+} currents and peak Ba^{2+} currents was 1.97 ± 1.43 nA ($n = 5$; $P < 0.05$ paired t-test). Both inactivation and activation were slower with Ba^{2+} than with Ca^{2+} as the current carrier. Although we cannot completely reject the possibility that some of the current differences may arise from differences in the amount of outward current contamination, the differences in kinetics of activation and inactivation suggest genuine ion-dependent properties of the same channel.

Voltage-dependent properties of the Ca^{2+} current

The Ca^{2+} current typically began activating at −35 mV, peaked between +5 and +20 mV, and extrapolated to reversal at around +70 mV (Fig. 2, *A2, B2,* and *C2*). As in many other preparations, the experimentally observed reversal potential was much lower than the theoretically expected one for Ca^{2+} (Hille 1992).

Activation

Conductance was calculated assuming that the channels are ohmic, using the following equation

$$g_{ion} = \frac{I_{ion}}{V - E_{ion}} \qquad (3)$$

where g is the conductance, I is the current measured, V is the voltage, and E is the reversal potential for Ca^{2+} estimated by extrapolation of the *I-V* curve. Because the real equilibrium potential for Ca^{2+} is probably higher, this may yield an overestimation of Ca^{2+} conductance. The voltage dependence of the Ca^{2+} current conductance was sigmoidal, typically beginning to activate at −40 mV, saturating at
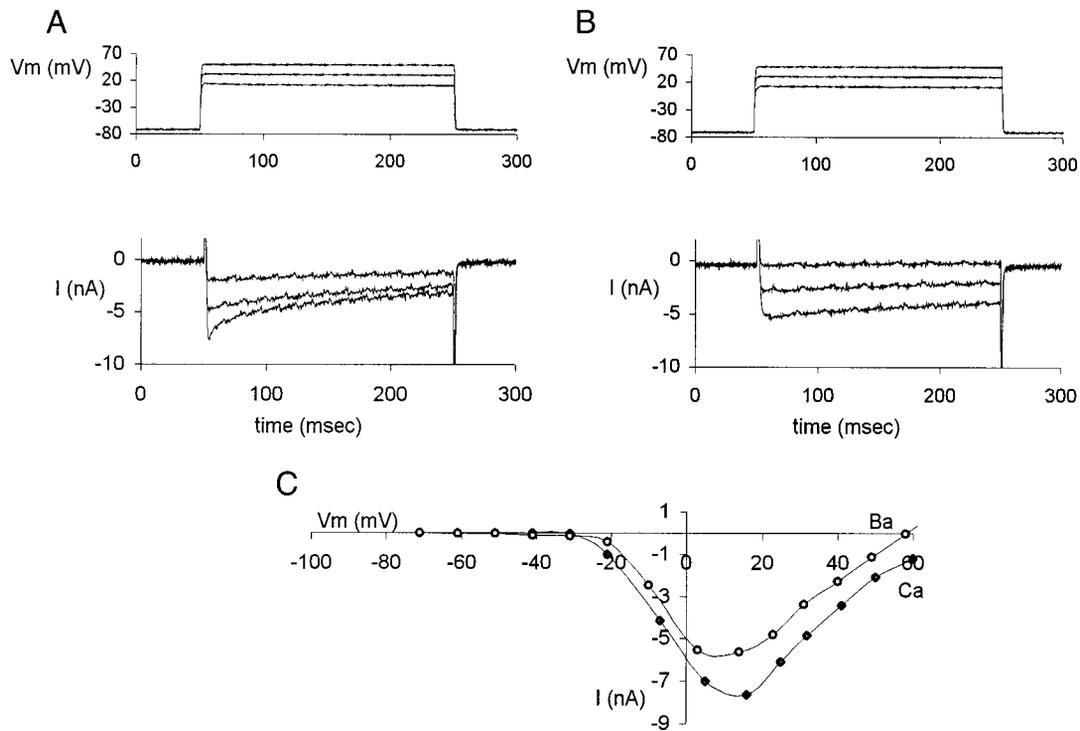
FIG. 3.   Currents carried by Ba^{2+} ions were smaller than Ca^{2+} currents and had slower activation and inactivation kinetics. *A*: a voltage-clamp experiment carried out in 11 mM Ca^{2+} ASW. *B*: currents elicited in 11 mM Ba^{2+} ASW in the same cell as in *A*. Note the smaller extent of inactivation. *C*: peak current-voltage relationship of the Ca^{2+} currents in *A* (◆) and of the Ba^{2+} currents in *B* (○).
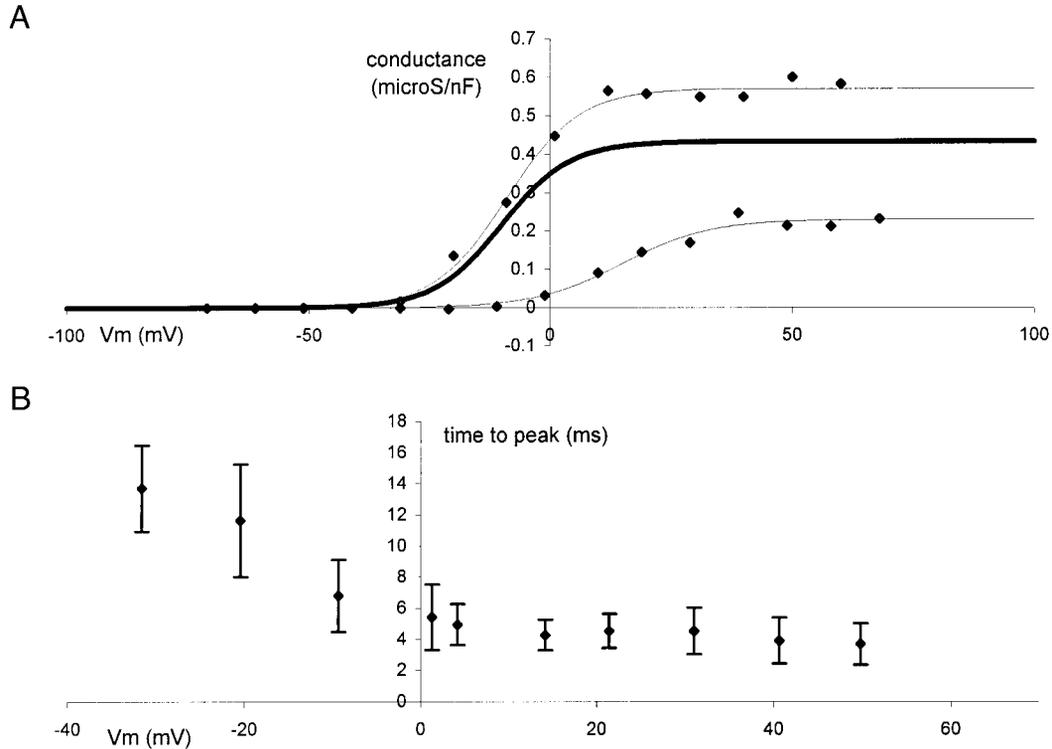
FIG. 4.   Voltage dependence of the L-type Ca^{2+} current activation. *A*: the voltage dependence of activation was sigmoidal, typically beginning to activate at about -40 mV, saturating at $+20$ mV and with half-activation at -10 mV. Symbols show data from 2 cells, thin lines are best fits of a Boltzman function and thick line is the mean Boltzman function pooled from 14 cells (see METHODS). Conductance was normalized to the cell's capacitance. *B*: time to peak of the L-type Ca^{2+} current decreased with depolarization, reaching values of <5 ms. Shown are means $\pm$ SD of 5 cells.

about $+20$ mV with half-activation at about -10 mV. Figure 4*A* shows two examples of a Boltzman function fitted to the activation data and the mean Boltzman function of 14 cells.

Conductance was normalized by dividing it by the capacitance. Maximum normalized conductance of the mean curve was 0.43 ± 0.21 (SD) μS/nF ($n = 14$; see METHODS), half-activation was at -10 ± 10 mV and the slope factor was 7 ± 2.4 mV. Activation of the Ca^{2+} current at the onset of the depolarizing step, as well as the deactivation at the end of the step, was very rapid. Time to peak of activation decreased as the voltage step became more positive, ranging from $\sim$15 ms at -30 mV to <5 ms at voltages greater than $+20$ mV (Fig. 4*B*). The activation kinetics were therefore too fast for accurate quantification. These fast kinetics also prevented the measurement of Ca^{2+} tail currents.

Inactivation

Inactivation of the inward current showed a complex, nonmonotonical voltage dependence. Steady-state inactivation was evaluated using a prepulse conditioning protocol (Fig. 5*A*). Inactivation began at about -45 mV, was maximal at about $+20$ mV and lessened at more positive voltages, thus showing a voltage dependence similar to the voltage dependence of the current itself (Fig. 5*B*). Inactivation thus seems to be current rather than voltage dependent, suggesting a Ca^{2+}-dependent inactivation mechanism. The fact that Ba^{2+} currents inactivate more slowly than Ca^{2+} currents also provides support for a Ca^{2+}-dependent inactivation mechanism. Ca^{2+}-dependent inactivation of L-type Ca^{2+} channels has been suggested for a variety of preparations, including the ARC muscle cells of *Aplysia* (Brezina et
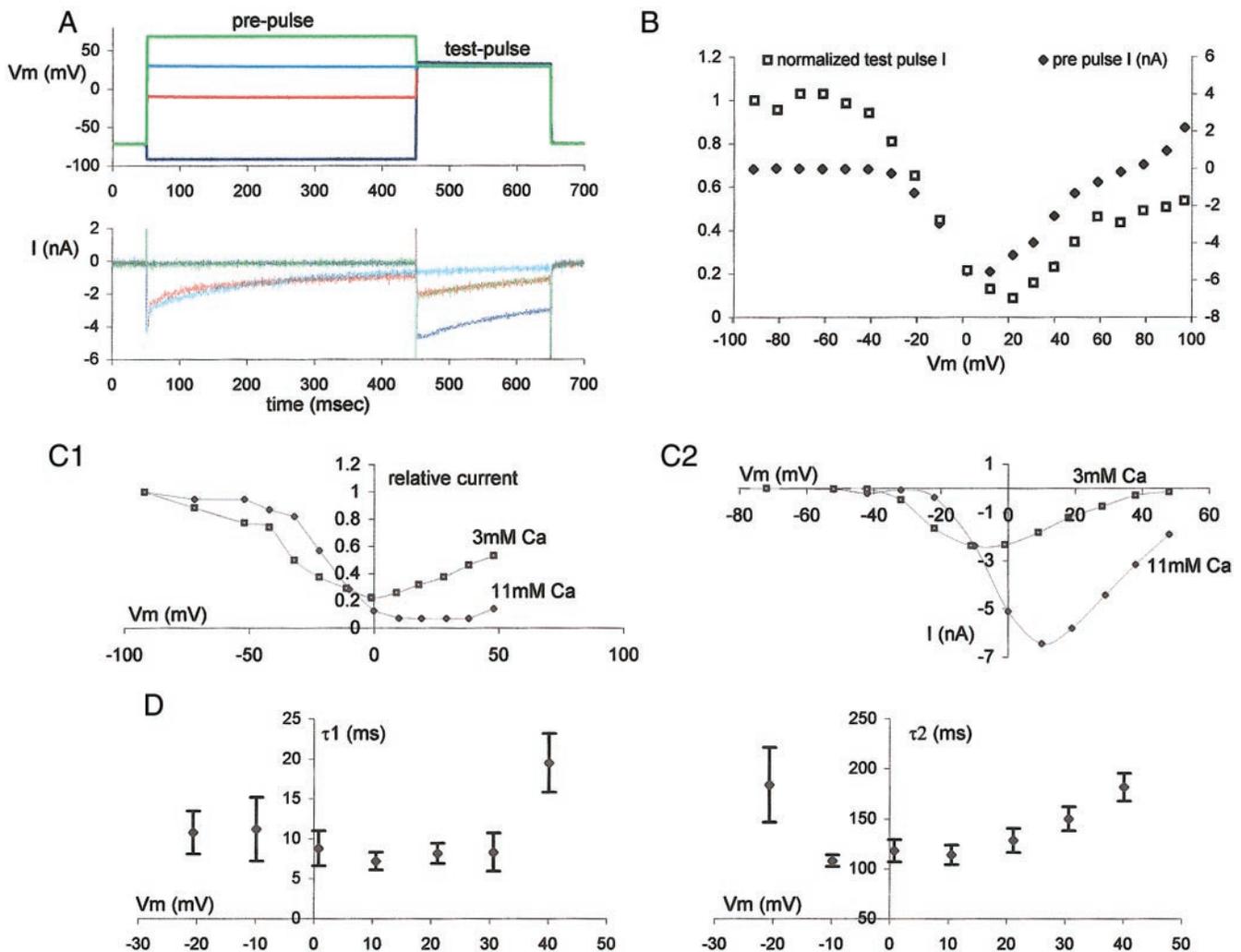

FIG. 5. Inactivation of the L-type Ca^{2+} current is Ca^{2+} dependent. *A*: the prepulse conditioning protocol used to evaluate inactivation. Matching voltage and current traces have the same color. Note that the green and blue current traces overlap during the prepulse but not during the test pulse (green and red traces overlap during the test pulse). *B*: voltage dependence of inactivation of the same cell as in *A*. Inactivation follows a course parallel to that of the current-voltage relationship. Filled diamonds, the peak current-voltage relationship of the inactivating prepulse. Open squares, the normalized peak current-voltage relationship of the test-pulse (test-pulse peak current was normalized to the current elicited after the lowest prepulse). *C1*: inactivation is altered when $[Ca^{2+}]_o$ is reduced to 3 mM. Inactivation is enhanced at negative voltages and reduced at positive voltages (see text). Filled diamonds, the normalized test-pulse peak current in 11 mM Ca^{2+}; open squares, the normalized test-pulse peak current in 3 mM Ca^{2+}. *C2*: prepulse peak current-voltage relationship of the same cell as in *C1*. Symbols as in *C1*. Note the similarity of cross point voltages in *C, 1* and *2* (see text). *D*: both time constants of inactivation show voltage dependence with minima at the voltage region where the Ca^{2+} current is maximal. Shown are means $\pm$ SD of 6 cells.

al. 1994c; Eckert and Ewald 1983b; Hille 1992; for a review see Eckert and Chad 1984).

The inward current during the inactivating prepulse did not, however, uniquely determine the amount of inactivation. Two prepulses eliciting the same prepulse peak currents (1 on each side of the *I-V* curve peak) resulted in different test-pulse currents, the more depolarizing prepulse causing greater inactivation (see example in Fig. 5*B*). This nonuniqueness may be due to outward current contamination in the descending part of the *I-V* curve (voltages more positive than the peak). That is, the actual amount of Ca^{2+} entering the cell may be larger than measured, thus explaining the large extent of inactivation. Or it may be due to some voltage dependence in addition to the Ca^{2+} dependence as has also been observed in snail neurons (Gutnick et al. 1989).

Inactivation followed a time course best described by two time constants: a fast time constant in the order of 10 ms and a slow time constant in the order of 150 ms. Both time constants were mildly voltage dependent and reached a minimum at a similar voltage to that of the maximal current (Fig. 5*D*).

To further check whether the inactivation is Ca^{2+} dependent, we measured inactivation of currents elicited in ASW containing 3 mM Ca^{2+}. If the inactivation of the Ca^{2+} current is indeed Ca^{2+} dependent, then lowering the external concentration of Ca^{2+} should result in a decrease in inactivation because currents will be smaller. Figure 5*C1* shows that inactivation was lower in 3 mM Ca^{2+} than in 11 mM Ca^{2+} at voltages more positive than −10 mV but was greater at more negative voltages.

The increase of inactivation at negative voltages is explained by shift in voltage dependence of the Ca^{2+} current at the two extracellular Ca^{2+} concentrations. Lowering the extracellular Ca^{2+} concentration from 11 to 3 mM resulted in a leftward shift in the activation curve of the Ca^{2+} current in all experiments (*n* = 3; Fig. 5*C2*). Ca^{2+} currents elicited in 3 mM Ca^{2+} were actually higher than those elicited in 11 mM Ca^{2+} at voltages negative to about −10 mV and thus caused more inactivation. Note that the cross points of the two curves in Fig. 5*C, 1* and *2,* are at the same voltage, indicating a direct correlation between the current magnitude and inactivation.

This shift in voltage dependent gating by external Ca^{2+} has been reported in almost all voltage-dependent channels (Formenti et al. 2001; Hille 1992; Johnson et al. 2001).

Characterization of the outward currents

Voltage steps applied in Mg-ASW, revealed a two peaked outward current (Fig. 6*A*, ↓). As this current was totally blocked when Na^+ was replaced with 460 mM TEA, it is most probably a K^+ current (Fig. 6*B*). The two components of this outward current were easily differentiated by their kinetics, their voltage dependence and their pharmacological sensitivity. They are a fast activating, fast inactivating A-type current (henceforth referred to as A-type current or I_A), and a slow activating current with slow and mild inactivation, characteristic for delayed rectifiers (henceforth referred to as delayed rectifier or I_K; Fig. 7*A, 1* and *2*). The properties of these two currents were very similar to those of A-type currents and delayed rectifiers in many other preparations (Brezina et al.1994b; Hille 1992; Rudy 1988).

The A-type K^+ current was totally blocked by 10 mM 4AP, whereas the delayed rectifier was totally blocked by 10 mM TEA (Fig. 7). This pharmacological difference was first used to study the two currents separately. However, as can be seen in Fig. 7*C1,* the algebraic sum of the two isolated currents was very different from the current recorded with no blockers in the bath. Either the A-type current was partially blocked by TEA or the delayed rectifier was partially blocked by 4AP or both.

To check this, we first tested the effect of 4AP on the delayed rectifier by applying depolarizing voltage steps from a holding potential of −40 mV. The A-type current was almost totally inactivated at this voltage (see Fig. 9*C2*). Application of 4AP reduced the steady state level of I_K to 63 ± 28% (mean ± SD, *n* = 5) of control values (data not shown). The sensitivity of I_K to 4AP was insufficient to explain the total difference between the algebraic sum of the isolated currents and the total unblocked K^+ current. We therefore concluded that I_A is also partially TEA sensitive and characterized it by subtracting the 4AP-insensitive current from the total K^+ current.

To correct for the effect of 4AP on I_K, the 4AP-insensitive current was normalized so that the current at the end of the
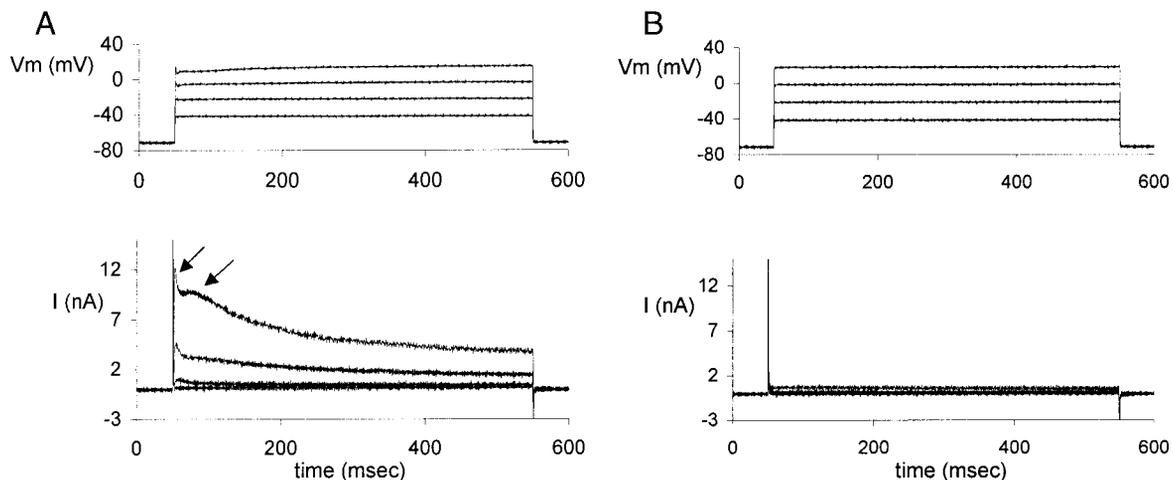

FIG. 6. Voltage steps elicited a 2-peak K^+ current when Ca^{2+} current was blocked. *A*: a voltage-clamp experiment using Mg-ASW as the bathing solution. Two peaks are evident in the current (↓). *B*: as both components of the outward current were blocked when Na^+ was replaced with 460 mM TEA in the bathing solution, these are K^+ currents.
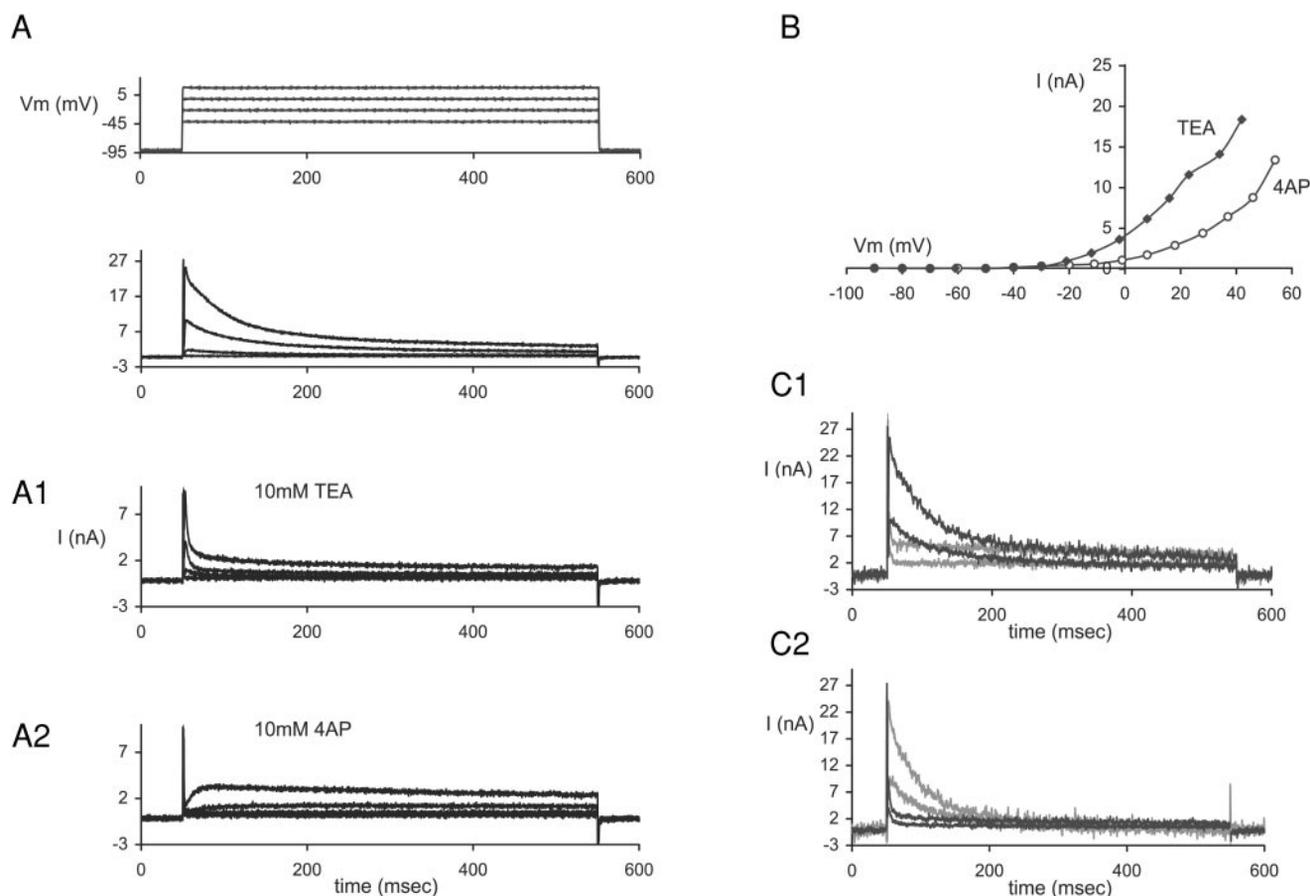
FIG. 7. Two components of the K^+ current are a fast-activating fast-inactivating A-type current and a slower-activating delayed rectifier, which inactivates slowly and mildly. *A*: voltage steps applied in Mg-ASW activated 2 K^+ currents. *A1*: 10 mM TEA blocked the delayed rectifier and revealed a transient A-type current. *A2*: 10 mM 4AP blocked the A-type current, revealing a slow-activating, sustained delayed rectifier. *B*: peak current-voltage relationship of the A-type current (filled diamonds) and the delayed rectifier (open circles). *C*: the A-type current is not insensitive to TEA. *C1*: the algebraic sum of TEA-insensitive current and the 4AP-insensitive current, shown in gray, does not reproduce the total unblocked current, shown in black. The results of 2 voltage steps are shown. *C2*: the A-type current isolated by subtraction of the delayed rectifier from the total outward current. Black traces are recordings in the presence of 10 mM TEA. Gray traces are the result of the subtraction.

voltage step was equal to the total K^+ current at the end of the step, assuming that the A-type current fully inactivated during a 500-ms step. The result of the subtraction showed a very different amplitude and time course from the current measured in the presence of TEA (Fig. 7*C2*). The A-type current is therefore sensitive to TEA. This sensitivity may also explain the very rapid inactivation of the current recorded in the presence of TEA. If TEA blocks only A-type channels that are open, the kinetics of the closure of this current in the presence of TEA actually reflect the kinetics of TEA blocking the current rather than the kinetics of inactivation.

Delayed rectifier K^+ current

To isolate the delayed rectifier from the A-type current, 10 mM 4AP was added to the Mg-ASW. As noted in the preceding text, this also reduced I_K to 63 $\pm$ 28% (mean $\pm$ SD, $n = 5$) of control current. Under these conditions, depolarizing voltage steps elicited a relatively slow-activating current with

slow and mild inactivation (Fig. 7*A2*). This current typically began to activate at about -35 mV and increased monotonically with depolarization. The activation curve of the delayed rectifier fitted a sigmoidal Boltzman function (see METHODS), half-activated at about $+25 \pm 15$ (SD) mV ($n = 6$) and extrapolated to saturation of 0.44 $\pm$ 0.2 μS/nF at about $+100$ mV (Fig. 8*A*). The slope factor was 17 $\pm$ 2.8 mV. Maximal conductance is probably higher because 10 mM 4AP blocked $\sim$40% of the delayed rectifier, as mentioned in the preceding text. Kinetics of activation were voltage dependent with time constant reaching a maximal value of $\sim$20 ms at $\sim$5 mV and decreasing at higher or lower voltages to $\sim$4 ms (Fig. 8*B*).

Steady-state inactivation was evaluated using the prepulse conditioning protocol as shown in Fig. 8*C1*. Voltage dependence of steady-state inactivation was sigmoidal, typically beginning at -60 mV and saturating at about $+60$ mV, where only 30 $\pm$ 22% ($n = 8$) of the current had inactivated (Fig. 8*C2*). The slope factor of the inactivation curve was 10 $\pm$ 8 mV. Inactivation kinetics were very variable and seemed to be voltage independent, average time constant was 152 $\pm$ 47 (SD) ms ($n = 5$).
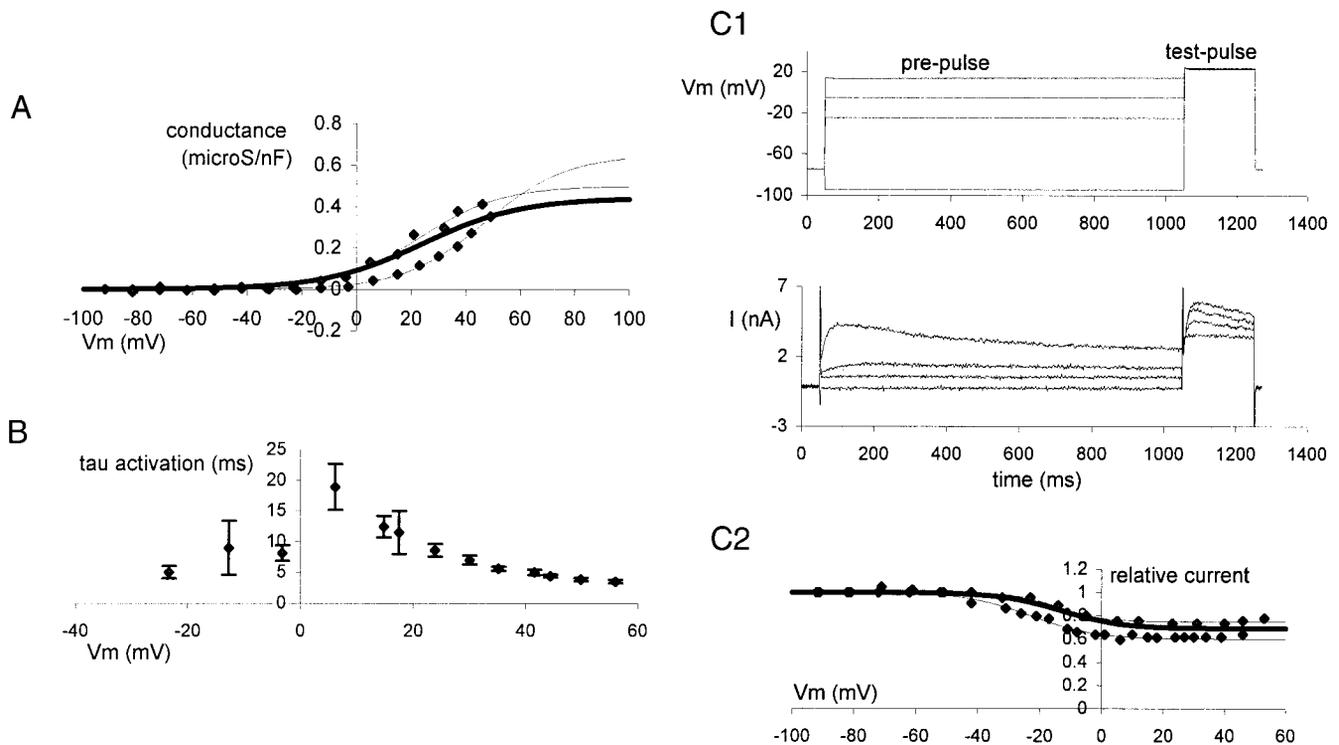
FIG. 8. Voltage dependence of the delayed rectifier. *A*: voltage dependence of activation of the delayed rectifier. Activation typically began at about −40 mV and extrapolated to saturation at ∼100 mV. Symbols are data from 2 cells, thin lines are the fit of a Boltzman function to these data, and thick line is the mean Boltzman function of 6 cells. *B*: activation time constant is voltage dependent, increasing with depolarization at negative voltages and decreasing with depolarization at positive voltages. Shown are mean ± SE of 6 cells. *C1*: a prepulse conditioning protocol used for evaluating steady-state inactivation. *C2*: voltage dependence of steady-state inactivation of the delayed rectifier is sigmoidal, beginning at about −40 mV and reaching saturation at ∼40 mV where only ∼30% of the current is inactivated. Symbols and lines as in *A*. Data from 8 cells are shown.

A-type K+ current

The A-type current typically began activating at about −60 mV and, like the delayed rectifier, increased monotonically as the depolarizing voltage steps became more positive. The activation curve of this current was also fitted by a Boltzman function (Fig. 9*A*). The current was half-activated at −3 ± 8 mV ($n = 7$), maximal conductance was $2.75 ± 0.7$ $\mu S/nF$, and the slope factor of the activation Boltzman was $11 ± 2$ mV. Activation was very rapid with time to peak of ∼12 ms at −35 mV, decreasing to ∼3 ms at higher voltages (Fig. 9*B*). These kinetics of activation were too rapid to allow accurate description.

Deactivation was also very rapid, preventing tail current recording. We used the prepulse conditioning protocol for steady-state inactivation analysis as in the previous experiments (Fig. 9*C1*). The A-type current was isolated pharmacologically in these experiments by adding 10 mM TEA to the Mg-ASW. Figure 9*C2* shows that inactivation of I_A fitted a Boltzman function. The A-type current was half inactivated at −51 ± 6 mV ($n = 7$), and saturated at 92 ± 0.07% inactivation. The mean slope factor of the inactivation Boltzman curve was $5 ± 2$ mV. The time constant of inactivation was evaluated by fitting a single exponent to the declining phase of the A-type current, which was obtained by subtracting the 4AP-insensitive current from the total K+ current after correcting for I_K block by 4AP as described in the preceding text.

Time constant of inactivation was mildly voltage dependent

with values ranging from ∼50 ms at −35 mV to ∼80 ms at −5 mV and steadily declining to ∼70 ms at +35 mV (Fig. 9*D*).

DISCUSSION

Ca^{2+} spikes have first been demonstrated in the muscle fibers of crustaceans (Fatt and Ginsborg 1958; Fatt and Katz 1953; Werman and Grundfest 1961), but most of these cells do not produce action potentials unless either K+ currents are partially blocked or extracellular Ca^{2+} is raised or Ca^{2+}-binding agents are injected into the cell (Hagiwara and Naka 1964). Blocking K+ currents also renders *Aplysia* ARC muscle cells (Brezina et al. 1994b) and muscle cells of the mollusk *Philine aperta* (Dorsett and Evans 1991) capable of generating action potentials. Ca^{2+} spikes generated by muscle cells in physiological conditions have been demonstrated in ascidian muscle (Greaves et al. 1996), in the radula opener muscle of *Aplysia* (Evans et al. 1996; Scott et al. 1997), and in vertebrate smooth muscle (Guyton 1991; Lang 1989). The obliquely striated muscle fibers of the earthworm also produce fast overshooting action potentials that are insensitive to TTX and strongly dependent on extracellular Ca^{2+} concentration (Hidaka et al. 1969a,b); however, the ionic currents underlying these action potentials have not been characterized.

The octopus arm muscle cells are an extreme example of muscle cells that generate fast (∼3 ms width at half height) overshooting action potentials in the absence of voltage-gated Na+ channels. Mature ascidian muscle cells show Ca^{2+} spikes of ∼10 ms (Greaves et al. 1996). Action potentials of verte-
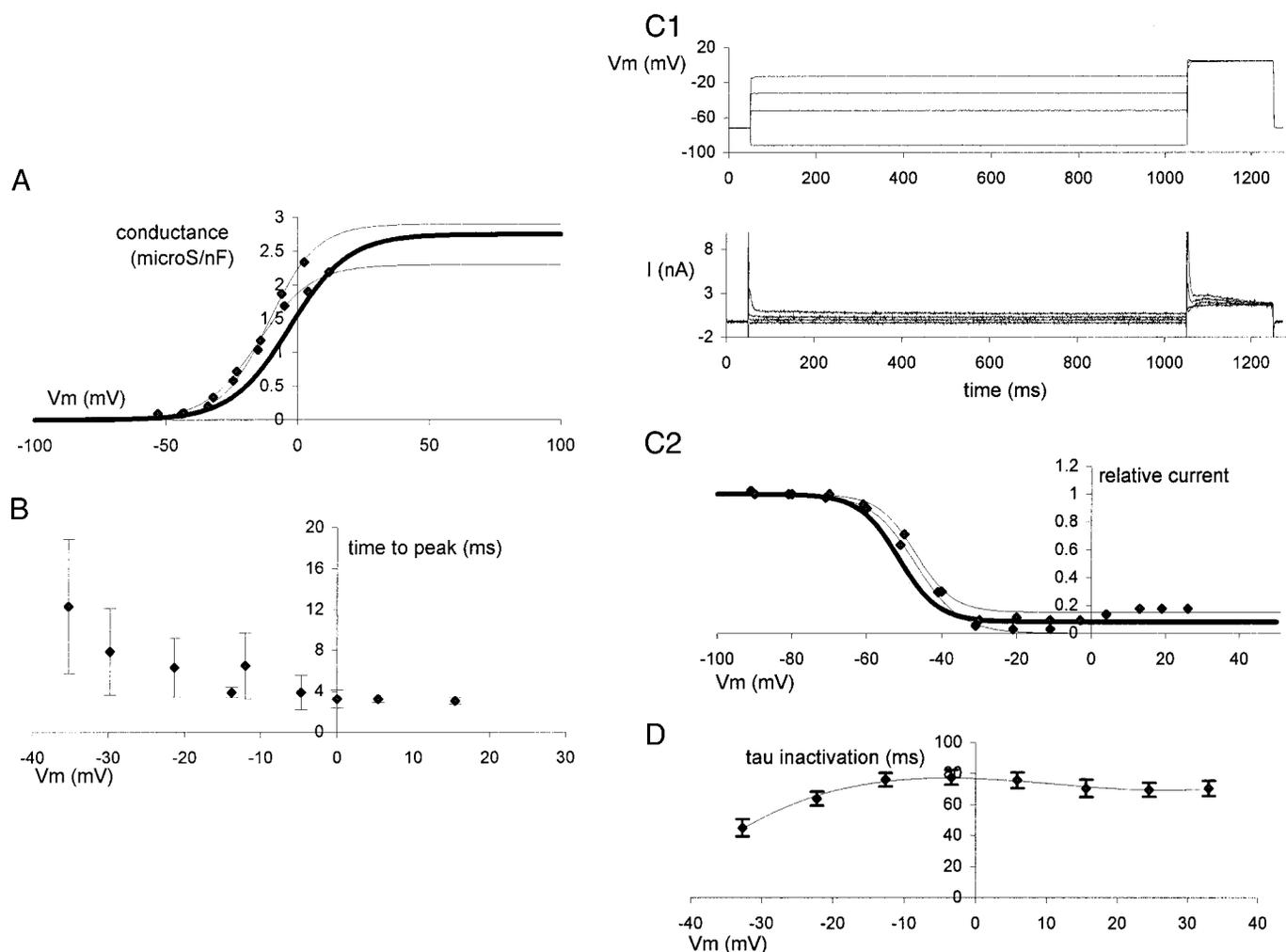
FIG. 9. Voltage dependence of activation and inactivation of the A-type current. *A*: voltage dependence of A-type current activation. This current typically began activating at about -40 mV and extrapolated to saturation at about $+40$ mV. Symbols show experimental data from 2 cells, thin lines show a Boltzman function fitted to these data and thick line shows the average activation curve of 7 cells. *B*: time to peak of the A-type current decreased with depolarization, reaching 3 ms at positive voltages. Shown are means $\pm$ SD of 15 cells. *C1*: a prepulse conditioning experiment used for evaluating the A-type current steady-state inactivation. I_A was isolated pharmacologically with 10 mM TEA in the bathing solution. *C2*: inactivation typically began at about -70 mV and was almost complete at about -30 mV. Symbols are as in *A*. *D*: time constant of inactivation of the A-type current is mildly voltage dependent, ranging from ~ 50 to ~ 80 ms. Shown are means $\pm$ SE of 6 cells.

brate smooth muscle cells range from tens to hundreds of milliseconds (Guyton 1991; Lang 1989).

In the octopus arm muscle, rapid overshooting spikes are generated both when current is directly injected to dissociated muscle fibers and in an innervated muscle preparation in response to synaptic input (Matzner et al. 2000), showing that these action potentials are generated in physiological conditions.

Categorization of the ionic currents of the octopus arm muscle cells and their likely roles in the generation of electrical activity

The muscle cells of the octopus arm display a broad range of excitable behaviors ranging from damped to accelerating oscillations, fast overshooting spike and Ca plateau potentials. In this study, we found three depolarization-activated ionic currents that contribute to this rich repertoire: a Ca^{2+} current, a transient K^+ current, and a sustained K^+ current. It cannot be ruled out that other currents, such as a Ca^{2+}-activated K^+

current participate in the generation of electrical responses; however, current-clamp experiments have shown that there is no long afterhyperpolarization at the end of action potentials (see also Matzner et al. 2000).

The Ca^{2+} current is activated at relatively depolarized voltages, has slow current-dependent inactivation, and is sensitive to nifedipine. While these properties are characteristic for L-type Ca^{2+} channels (Carbone and Swandulla 1989; Hille 1992), the Ca^{2+} current did not show higher conductivity to Ba^{2+} than to Ca^{2+} ions, also a defining property of the L-type Ca^{2+} channel. Overall, however, this Ca^{2+} current appears to belong to the high-voltage-activated L-type currents found in many mulluscan excitable cells (Brezina et al. 1994c; Chrachri and Williamson 1997; Gutnick et al. 1989; Laurienti and Blankenship 1996; Rogers et al. 1997; Scott et al. 1997) as well as in other invertebrate excitable cells (Salkoff and Wyman 1983; Yeomen et al. 1999).

The transient K^+ current activated very rapidly and was

fully inactivated in ~200 ms; it was blocked by 10 mM 4AP but was less sensitive to similar concentrations of TEA. Steady-state inactivation of this current began at about -80 mV and was almost complete at -40 mV. This thus appears to be an A-type K^+ current as also found in many other invertebrate preparations (Brezina et al. 1994b; Chrachri and Williamson 1997; Dorsett and Evans 1991; Hille 1992; Laurienti and Blankenship 1996; Rudy 1988; Salkoff and Wyman 1983; Scott et al. 1997; Yeoman and Benjamin 1999).

The sustained K^+ current was categorized as a member of the delayed rectifier family because of its relatively slow activation kinetics, slow and mild inactivation, and its higher sensitivity to TEA than to 4AP (Brezina et al.1994b; Chrachri and Williamson 1997; Dorsett and Evans 1991; Hille 1992; Laurienti and Blankenship 1996; Rudy 1988; Salkoff and Wyman 1983; Scott et al. 1997). The delayed rectifier began activating at membrane potentials similar to those where the A-type current began activating but reached maximal conductance of lower values and at more depolarized voltage. Steady-state inactivation of this current began where the A-type current was practically fully inactivated (approximately -40 mV).

Because the fast-activating slow-inactivating L-type Ca^{2+} current is the sole inward current carrier, it is obviously responsible for the generation of all regenerative electrical responses. Its slow inactivation also implies that unlike most Na^+ spikes the fast termination of excitable phenomena depends on the activation of outward currents. That is, the shape and duration of action potentials is determined by K^+ currents. Classically, the role of terminating action potentials is attributed to delayed rectifier currents, whereas that of spacing action potentials within a spike train is attributed to A-type currents (Connor and Stevens 1971; Hille 1992). The delayed rectifier does most probably terminate action potentials in the octopus arm muscle cells. When the muscle cells were held at -35 mV by DC current injection, fast action potentials of normal duration were generated, although the A-type current was almost totally inactivated (data not shown). Ca^{2+}-activated K^+ currents might also terminate action potentials. However, these currents are usually activated relatively slowly and thus seem unlikely to terminate such fast action potentials. Yet they might play a role in the generation of other types of electrical phenomena.

Likely roles of the electrical activity in contraction of the octopus arm muscle cells

The wide range of regenerative responses suggests that the ionic currents in these cells are susceptible to activity-dependent changes. However, overshooting neuronal-like action potentials are much more frequent than other responses when the cells are both directly stimulated with current injection and activated by synaptic input (see also Matzner et al. 2000). Therefore the generation of action potentials appears most important for understanding the control of muscle activation in the octopus arm.

Action potentials are generated when a relatively high-threshold voltage of -30 mV is reached. Single presynaptic action potentials can generate such depolarization because the innervation of these cells includes a class of inputs of exceptionally high quantal amplitude (5–25 mV) (Matzner et al. 2000).

The overshooting action potentials are most likely not involved in propagating activity along the muscle cell as the cells are electrically very compact, and there is no indication for significant electrical coupling between them (Matzner et al. 2000). Thus it may be postulated that rapid Ca^{2+} action potentials serve two purposes in these unique muscle cells. First, action potentials with these properties (fast, not accommodating) might enable control of muscle activation by controlling the firing rate. The spike train frequency and duration will follow with high fidelity the magnitude and duration of the synaptic input. Second, action potentials might also be an efficient mechanism for rapidly introducing large amounts of Ca^{2+} into the cell. This would be especially feasible if a large amount of Ca^{2+} were to enter as a tail current (Spencer et al. 1989), but because the Ca^{2+} current in these cells deactivates very rapidly, Ca^{2+} tail currents seem unlikely. The excitation-contraction mechanism in cephalopod muscle is still unknown, and it is not clear whether contraction is activated by extracellular Ca^{2+} influx or by Ca^{2+} release from intracellular stores. However, in most cephalopod muscles, contraction is abolished when Ca^{2+} is omitted from the extracellular solution (Bone et al. 1995). Furthermore these small diameter cells lack any transverse tubular-like system to transmit the electrical signal into the core of the cell (Bone et al. 1995) and therefore they may have evolved a novel mechanism of using a large Ca^{2+} action potential for introducing Ca^{2+} via the sarcolemma.

REFERENCES

BONE Q, BROWN ER, AND USHER M. The structure and physiology of cephalopod muscle fibers. In: *Cephalopod Neurobiology*, edited by Abbot NJ, Williamson R, and Maddock L. New York: Oxford Science Press, 1995, p. 301–329.

BREZINA V, EVANS CG, AND WEISS KR. Characterization of the membrane ion currents of a model molluscan muscle, the accessory radula closer muscle of *Aplysia californica*. I. Hyperpolarization-activated currents. *J Neurophysiol* 71: 2093–2112, 1994a.

BREZINA V, EVANS CG, AND WEISS KR. Characterization of the membrane ion currents of a model molluscan muscle, the accessory radula closer muscle of *Aplysia californica*. II. Depolarization-activated K currents. *J Neurophysiol* 71: 2113–2125, 1994b.

BREZINA V, EVANS CG, AND WEISS KR. Characterization of the membrane ion currents of a model molluscan muscle, the accessory radula closer muscle of *Aplysia californica*. III. Depolarization-activated Ca currents. *J Neurophysiol* 71: 2126–2138, 1994c.

CARBONE E AND SWANDULLA D. Neuronal calcium channels: kinetics, blockade and modulation. *Prog Biophys Mol Biol* 54: 31–58, 1989.

CHRACHRI A AND WILLIAMSON R. Voltage-dependent conductance in cephalopod primary sensory hair cells. *J Neurophysiol* 78: 3125–3132, 1997.

CONNOR JA AND STEVENS CF. Prediction of repetitive firing behaviour from voltage clamp data on an isolated neurone soma. *J Physiol (Lond)* 213: 31–53, 1971.

DORSETT DA AND EVANS CG. Potassium and calcium currents in dissociated muscle fibers of the mollusk *Philine aperta. J Exp Biol* 155: 305–321, 1991.

ECKERT R AND CHAD JE. Inactivation of Ca channels. *Prog Biophys Mol Biol* 44: 215–267, 1984.

ECKERT R AND EWALD D. Calcium tail currents in voltage-clamped intact nerve cell bodies of *Aplysia californica. J Physiol (Lond)* 345: 533–548, 1983a.

ECKERT R AND EWALD D. Inactivation of calcium conductance characterized by tail current measurements in neurons of *Aplysia californica. J Physiol (Lond)* 345: 549–565, 1983b.

EVANS CG, ROSEN S, KUPFERMANN I, WEISS KR, AND CROPPER EC. Characterization of a radula opener neuromuscular system in *Aplysia. J Neurophysiol* 76: 1267–1281, 1996.

FATT P AND GINSBORG BL. The ionic requirements for the production of action potentials in crustacean muscle fibers. *J Physiol (Lond)* 142: 516–543, 1958.

FATT P AND KATZ B. The electrical properties of crustacean muscle fibers. *J Physiol (Lond)* 120: 171–204, 1953.

FORMENTI A, DE SIMONI A, ARRIGONI E, AND MARTINA M. Changes in extracellular Ca^{2+} can affect the pattern of discharge in rat thalamic neurons. *J Physiol (Lond)* 535: 1: 33–45, 2001.

GILLY WF, PREUSS T, AND MCFARLANE MB. All-or-none contraction and sodium channels in a subset of sircular muscle fibers of squid mantle. *Biol Bull* 191: 337–340, 1996.

GREAVES AA, DAVIS AK, DALLMAN JE, AND MOODY WJ. Co-ordinated modulation of Ca^{2+} and K^+ currents during ascidian muscle development. *J Physiol (Lond)* 497: 39–52, 1996.

GUTFREUND Y, FLASH T, FIORITO G, AND HOCHNER B. Patterns of arm muscle activation involved in octopus reaching movements. *J Neurosci* 18: 5976–5987, 1998.

GUTFREUND Y, FLASH T, YAROM Y, FIORITO G, SEGEV I, AND HOCHNER B. Organization of octopus arm movements: a model system for studying the control of flexible arms. *J Neurosci* 16: 7297–7307, 1996.

GUTNICK MJ, LUX HD, SWANDULLA D, AND ZUCKER H. Voltage-dependent and calcium-dependent inactivation of calcium channel current in identified snail neurons. *J Physiol (Lond)* 412: 197–220, 1989.

GUYTON AC. *Textbook of Medical Physiology* (8th ed.). Philadelphia, PA: Saunders, 1991.

HAGIWARA S AND NAKA KI. The initiation of spike potential in barnacle muscle fibers under low extracellular Ca^{2+}. *J Gen Physiol* 48: 141–162, 1964.

HIDAKA T, ITO Y, AND KURIYAMA H. Membrane properties of the somatic muscle (obliquely striated muscle) of the earthworm. *J Exp Biol* 50: 387–403, 1969a.

HIDAKA T, ITO Y, KURIYAMA H, AND TASHIRO N. Effects of various ions on the resting and active membrane of the somatic muscle of the earthworm. *J Exp Biol* 50: 405–415, 1969b.

HILLE B. *Ionic Channels of Excitable Membranes* (2nd ed.). Sunderland, MA: Sinauer, 1992.

HINES ML AND CARNEVALE NT. The NEURON simulation environment. *Neural Comput* 9: 1179–1209, 1997.

JOHNSON JP JR, BALSER JR, AND BENNETT PB. A novel extracellular calcium sensing mechanism in voltage gated potassium ion channels. *J Neurosci* 21: 4143–4153, 2001.

KIER WM. The musculature of squid arms and tentacles: ultrastructural evidence for functional differences. *J Morphol* 185: 223–239, 1985.

KIER WM AND SMITH KK. Tongues, tentacles and trunks: the biomechanics of movement in muscular-hydrostats. *Zool J Linn Soc* 83: 307–324, 1985.

LANG RJ. Identification of the major membrane currents in freshly dispersed single smooth muscle cells of guinea pig ureter. *J Physiol (Lond)* 412: 375–395, 1989.

LAURIENTI PJ AND BLANKENSHIP JE. Parapodial swim muscle in *Aplysia braziliana*. I. Voltage-gated membrane currents in isolated muscle fibers. *J Neurophysiol* 76: 1517–1530, 1996.

LLINAS R, STEINBERG IZ, AND WALTON K. Presynaptic calcium currents in squid giant synapse. *Biophys J* 33: 289–322, 1981.

LOWY J AND MILLMAN BM. Mechanical properties of smooth muscles of cephalopod mollusks. *J Physiol (Lond)* 160: 353–363, 1962.

MATZNER H, GUTFREUND Y, AND HOCHNER B. Neuromuscular system of the flexible arm of the octopus: physiological characterization. *J Neurophysiol* 83: 1315–1328, 2000.

MILLIGAN BJ, CURTIN NA, AND BONE Q. Contractile properties of obliquely striated muscle from the mantle of squid (*Alloteuthis subulata*) and cuttlefish (*Sepia officinalis*). *J Exp Biol* 200: 2425–2436, 1997.

O'DOR RK. Limitations on locomotor performance in squid. *J Appl Physiol* 64: 128–134, 1988.

PROSSER CL AND YOUNG JZ. Responses of muscles of the squid to repetitive stimulation of the giant nerve fibers. *Biol Bull* 73: 237–241, 1937.

ROGERS CM, NELSON L, MILLIGAN BJ, AND BROWN ER. Different excitation-contraction coupling mechanisms exist in squid, cuttlefish, and octopod mantle muscle. *J Exp Biol* 200: 3033–3041, 1997.

RUDY B. Diversity and ubiquity of K channels. *Neuroscience* 25: 729–749, 1988.

SALKOFF LB AND WYMAN RJ. Ion currents in *Drosophila* flight muscles. *J Physiol (Lond)* 337: 687–709, 1983.

SCOTT ML, BREZINA V, AND WEIZZ KR. Ion currents and mechanisms of modulation in the radula opener muscle of *Aplysia. J Neurophysiol* 78: 2372–2387, 1997.

SPENCER AN, PRZYSIEZNIAK J, ACOSTA-URQUIDI J, AND BASARSKY TA. Presynaptic spike broadening reduces junctional potential amplitude. *Nature* 340: 636–639. 1989.

SUMBRE G, GUTFREUND Y, FIORITO G, FLASH T, AND HOCHNER B. Control of octopus arm extension by a peripheral motor program. *Science* 293: 1845–1848, 2001.

WERMAN R AND GRUNDFEST H. Graded and all-or-none electrogenesis in arthropod muscle. II. The effect of alkali-earth and onium ions on lobster muscle fibers. *J Gen Physiol* 44: 997–1027, 1961.

YEOMAN MS AND BENJAMIN PR. Two types of voltage-gated K^+ currents in dissociated heart ventricular muscle cells of the snail *Lymnaea stagnalis. J Neurophysiol* 82: 2415–2427, 1999.

YEOMAN MS, BREZDEN BL, AND BENJAMIN PR. LVA and HVA Ca^{2+} currents in ventricular muscle cells of the *Lymnaea* heart. *J Neurophysiol* 82: 2428–2440, 1999.